International Journal of Thermophysics, Vol. 24, No. 6, November 2003 (© 2003)

Evaluation of the Heat Leakage in the Thermal Diffusivity Measurement of Molten Metals by a Laser Flash Method

T. Nishi,[1,2] H. Ohta,[3] H. Shibata,[4] and Y. Waseda[4]

Received March 17, 2003

Evaluation of the radiative and conductive heat loss from a molten metal sample to the cell has been made in order to obtain accurate thermal diffusivities of molten metals at high temperature with a laser flash method. The results suggest that thermal diffusivity values of molten nickel can be determined in the temperature range from 1728 to 1928 K with an uncertainty of $\pm 3\%$ in comparison with case considering only the effect of radiative heat loss. The usefulness of a cell for a laser flash method has been confirmed by applying simulated results to evaluate the heat leakage in the thermal diffusivity measurement of molten metals.

KEY WORDS: heat loss; laser flash method; molten nickel; numerical analysis; thermal diffusivity.

1. INTRODUCTION

The thermal diffusivity of molten metals at high temperature are of importance in casting of metals and designing various plants using heat transfer fluids for fusion reactors, breeder reactors, and thermal energy storage systems. The laser flash method is recognized as one of the most powerful techniques to measure the thermal diffusivity of molten metals at high temperature when a precise sample thickness is available. For this purpose, several types of cells have been developed [1, 2].

[1] Graduate School, Department of Materials Processing, Tohoku University, Sendai 980-8577, Japan.
[2] To whom correspondence should be addressed. E-mail: nishi@mail.tagen.tohoku.ac.jp
[3] Department of Materials Science, Ibaraki University, Hitachi 316-8511, Japan.
[4] Institute of Multidisciplinary Research for Advanced Materials, Tohoku University, Sendai 980-8577, Japan.

0195-928X/03/1100-1735/0 © 2003 Plenum Publishing Corporation

Recent measured values of the thermal diffusivity of molten copper [3] using the laser flash method are found to be smaller than a frequently used reference value [4], and the heat leakage is suggested as a possible origin of such a difference. However, no analysis has been carried out with respect to the effect of heat loss from a molten metal sample to the cell at high temperature.

For the laser flash method for molten metals at temperatures higher than 1500 K, a simple cell has recently been developed by the present authors [5]. Then, the main purpose of this work is to estimate the effect of the radiative and conductive heat losses at the interface between the molten metals and the cell materials, and the experimental uncertainty will be analyzed using the measured thermal diffusivity values of molten nickel at high temperatures.

2. EXPERIMENTAL

The newly developed cell and apparatus are shown in Fig. 1 [5]. This cell consisted of three layers. The top and bottom were made of sapphire disks, which were transparent for laser beam and infrared ray. The cell wall was made of an alumina tube, and the molten metal was sandwiched between the two sapphire disks as shown in Fig. 1. The entire cell was compressed with the graphite fixture to suppress the volume expansion of the metal due to the phase transition from the solid to the molten state, i.e., to obtain an accurate sample thickness of the molten metal at elevated

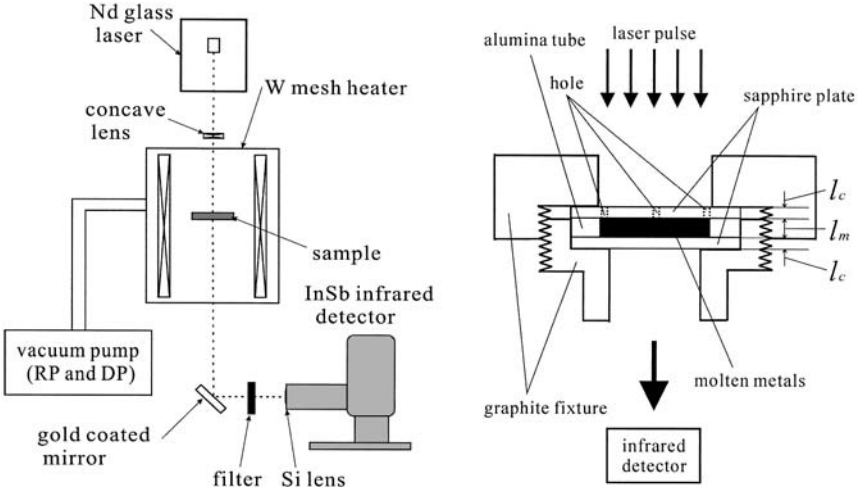

Fig. 1. Schematic diagram of a laser flash apparatus and sample cell.

temperatures. Four small holes in the upper sapphire plate work as a buffer to minimize the volume expansion of the molten metal and to have a residual gas inside the sample.

The front surface of the molten metal is subjected to a single pulse from a laser beam through the upper sapphire disk. The resulting temperature rise of the sample is measured with an infrared detector through the lower sapphire disks, and the thermal diffusivity value is estimated from the temperature response curve.

3. NUMERICAL MODEL FOR THERMAL DIFFUSIVITY ANALYSIS OF MOLTEN METALS

Under the present experimental conditions, the conductive heat loss at the interface must be taken into account quantitatively along with the radiative heat loss.

A schematic diagram of the configuration of the cell assembly is shown in Fig. 2. The following conditions are assumed to establish the heat transport equation governing the heat transport phenomena in the cell with the appropriate boundary and initial conditions:

(1) one-dimensional heat flow,

(2) the whole cell is under adiabatic conditions for the conductive heat flow,

(3) each layer is homogeneous,

(4) all thermophysical properties of the three layers are known,

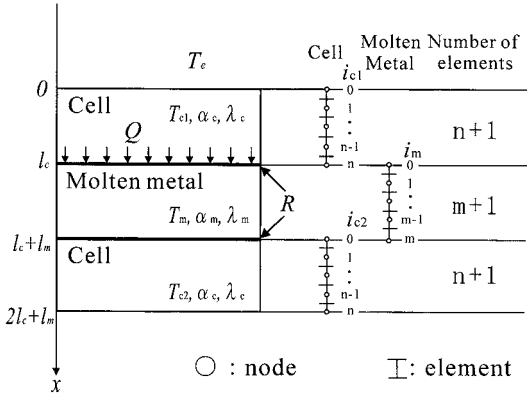

Fig. 2. Schematic diagram of the geometry of a three-layered cell.

(5) the thermal contact resistance at the interface between layers is uniform and has the same value at both the upper interface and the lower interface,

(6) the heat pulse is uniformly absorbed on the front surface,

(7) the radiative heat loss is proportional to the temperature difference, $T_m - T_e$,

(8) there is no absorption of the energy in the medium of the cell because the cell is transparent to both the laser pulse and infrared, and

(9) radiative heat loss occurs only on the surface of the molten metal.

The heat conduction equation for each layer is mathematically described in the following equations:

$$\frac{\partial^2 T_{c1}}{\partial x^2} - \frac{1}{\alpha_c}\frac{\partial T_{c1}}{\partial t} = 0 \tag{1}$$

$$\frac{\partial^2 T_m}{\partial x^2} - \frac{1}{\alpha_m}\frac{\partial T_m}{\partial t} = 0 \tag{2}$$

$$\frac{\partial^2 T_{c2}}{\partial x^2} - \frac{1}{\alpha_c}\frac{\partial T_{c2}}{\partial t} = 0 \tag{3}$$

The boundary conditions are given as shown below.

At the top of the upper sapphire disk,

$$\left[\frac{\partial T_{c1}}{\partial x}\right]_{x=0} = 0 \tag{4}$$

At the bottom of the upper sapphire disk,

$$\left[\lambda_c \frac{\partial T_{c1}}{\partial x} - \frac{1}{R}(T_{c1} - T_m)\right]_{x=(l_c)_-} = 0 \tag{5}$$

At the top of the molten metal,

$$\left[\lambda_m \frac{\partial T_m}{\partial x} - \frac{1}{R}(T_{c1} - T_m) + 4\varepsilon\sigma T_e^3 (T_m - T_e)\right]_{x=(l_c)_+} = 0 \tag{6}$$

At the bottom of the molten metal,

$$\left[\lambda_m \frac{\partial T_m}{\partial x} - \frac{1}{R}(T_m - T_{c2}) - 4\varepsilon\sigma T_e^3 (T_m - T_e)\right]_{x=(l_c+l_m)_-} = 0 \tag{7}$$

At the top of the lower sapphire disk,

$$\left[\lambda_c \frac{\partial T_{c2}}{\partial x} - \frac{1}{R}(T_m - T_{c2})\right]_{x=(l_c+l_m)_+} = 0 \tag{8}$$

At the bottom of the lower sapphire disk,

$$\left[\lambda_c \frac{\partial T_{c2}}{\partial x}\right]_{x=2l_c+l_m} = 0 \tag{9}$$

where T is the temperature increase, α is the thermal diffusivity, λ is the thermal conductivity, R is the thermal contact resistance, l is the thickness, ε is the thermal emissivity of the surface of the sample, σ is the Stefan–Boltzmann constant, and T_e is the steady-state temperature. The subscripts c and m refer to the cell and molten metal, respectively. The subscripts $c1$ and $c2$ denote the upper sapphire layer and the lower layer, respectively. When t is 0, arbitrarily the energy, Q (see Fig. 2) is absorbed on the front surface of the sample.

The following dimensionless parameters are also introduced for simplification;

$$\alpha_c^+ = \frac{\alpha_c}{\alpha_m}, \quad t^+ = \frac{\alpha_m t}{l_m^2}, \quad \lambda_c^+ = \frac{\lambda_c}{\lambda_m}, \quad x^+ = \frac{x}{l_m},$$
$$l_c^+ = \frac{l_c}{l_m}, \quad R^+ = \frac{\lambda_m R}{l_m}, \quad Y = \frac{4\varepsilon\sigma T e^3 l_m}{\lambda_m} \tag{10}$$

The contribution of the radiative heat loss is expressed by a dimensionless parameter called a Biot number, Y, for the front and back surfaces of the molten metal. The normalized heat conduction equation for each layer is given below.

$$\frac{\partial^2 T_{c1}}{\partial x^+} - \frac{1}{\alpha_c^+}\frac{\partial T_{c1}}{\partial t^+} = 0 \tag{11}$$

$$\frac{\partial^2 T_m}{\partial x^+} - \frac{\partial T_m}{\partial t^+} = 0 \tag{12}$$

$$\frac{\partial^2 T_{c2}}{\partial x^+} - \frac{1}{\alpha_c^+}\frac{\partial T_{c2}}{\partial t^+} = 0 \tag{13}$$

The normalized boundary conditions are as follows:

$$\left[\frac{\partial T_{c1}}{\partial x^+}\right]_{x^+=0} = 0 \tag{14}$$

$$\left[\lambda_c^+ \frac{\partial T_{c1}}{\partial x^+} - \frac{1}{R^+}(T_{c1} - T_m)\right]_{x^+=(l_c^+)_-} = 0 \tag{15}$$

$$\left[\frac{\partial T_m}{\partial x^+} - \frac{1}{R^+}(T_{c1} - T_m) + Y(T_m - T_e)\right]_{x^+=(l_c^+)_+} = 0 \tag{16}$$

$$\left[\frac{\partial T_m^+}{\partial x^+} - \frac{1}{R^+}(T_m - T_{c2}) - Y(T_m - T_e)\right]_{x^+=(l_c^+ + 1)_-} = 0 \tag{17}$$

$$\left[\lambda_c^+ \frac{\partial T_{c2}}{\partial x^+} - \frac{1}{R^+}(T_m - T_{c2})\right]_{x^+=(l_c^+ + 1)_+} = 0 \tag{18}$$

$$\left[\frac{\partial T_{c2}}{\partial x^+}\right]_{x^+=2l_c^+ + 1} = 0 \tag{19}$$

As shown in Fig. 2, these equations for heat transfer are solved using numerical analysis, Eqs. (11) to (19) should be transformed into the finite difference form of temperature as shown below.

$$T_{c1}(0, j+1) = (1-2F_c)\, T_{c1}(0, j) + 2F_c T_{c1}(1, j) \tag{20}$$

$$T_{c1}(i_{c1}, j+1) = T_{c1}(i_{c1}, j) + F_c[T_{c1}(i_{c1}+1, j) + T_{c1}(i_{c1}-1, j) - 2T_{c1}(i_{c1}, j)] \quad (1 \leqslant i_{c1} \leqslant n-1) \tag{21}$$

$$T_{c1}(n, j+1) = T_{c1}(n, j) + 2F_c[T_{c1}(n-1, j) + T_{c1}(n, j)] - \frac{2\alpha_c^+ \, \Delta t^+ n}{R^+ \lambda_c^+ l_c^+}[T_{c1}(n, j) - T_m(0, j)] \tag{22}$$

$$T_m(0, j+1) = T_m(0, j) + \frac{2\,\Delta t^+ m}{R^+}[T_{c1}(n, j) - T_m(0, j)] - 2Y\,\Delta t^+ m[T_m(0, j) - T_e] - 2F_m[T_m(0, j) - T_m(1, j)] \tag{23}$$

$$T_m(i_m, j+1) = T_m(i_m, j) + F_m[T_m(i_m+1, j) + T_m(i_m-1, j) - 2T_m(i_m, j)] \quad (1 \leqslant i_m \leqslant m-1) \tag{24}$$

$$T_m(m, j+1) = T_m(m, j) + \frac{2\,\Delta t^+ m}{R^+}[T_{c2}(0, j) - T_m(m, j)] - 2Y\,\Delta t^+ m[T_m(m, j) - T_e] + 2F_m[T_m(m-1, j) - T_m(m, j)] \tag{25}$$

$$T_{c2}(0, j+1) = T_{c2}(0, j) + 2F_c[T_{c2}(0, j) + T_{c2}(1, j)] - \frac{2\alpha_c^+ \Delta t^+ n}{R^+ \lambda_c^+ l_c^+}[T_{c2}(0, j) - T_m(m, j)] \quad (26)$$

$$T_{c2}(i_{c2}, j+1) = T_{c2}(i_{c2}, j) + F_c[T_{c2}(i_{c2}+1, j) + T_{c2}(i_{c2}-1, j) - 2T_{c2}(i_{c2}, j)] \quad (1 \leqslant i_{c2} \leqslant n-1) \quad (27)$$

$$T_{c2}(n, j+1) = (1-2F_c)\, T_{c2}(n, j) + 2F_c T_{c2}(n-1, j) \quad (28)$$

where $F_c = \alpha_c^+ \Delta t^+/(l_c^+/n)$ and $F_m = \alpha_m^+ \Delta t^+/(1/m)$ are grid Fourier numbers of the cell and molten metals. i_{c1}, i_m, and i_{c2} are node numbers of the upper sapphire layer, the molten metal, and the lower sapphire layer, respectively. Δt^+ is the normalized resolution of time, j is the time step, $j+1$ and refers to a time Δt^+ later than j.

The essential points of the conventional thermal diffusivity analysis, considering only the effect of radiative heat loss, are summarized in the Appendix for convenience of the discussion.

4. THEORETICAL TEMPERATURE RESPONSE CURVE OF MOLTEN METALS

The theoretical temperature response curves of the rear surface of the sample are shown in Fig. 3. Dimensionless parameters α_c^+, l_c^+, and λ_c^+ are introduced by using heat transfer property values and sizes of sapphire and molten nickel. The values of the specific heat, thermal diffusivity, and density of sapphire at 2000 K used here were $1340\ \mathrm{J \cdot kg^{-1} \cdot K^{-1}}$ [6], $1.15 \times 10^{-6}\ \mathrm{m^2 \cdot s^{-1}}$ [6], and $3800\ \mathrm{kg \cdot m^{-3}}$ [6], respectively. On the other hand, the values of the specific heat, thermal diffusivity, and density of molten nickel at 1828 K used here are $656\ \mathrm{J \cdot kg^{-1} \cdot K^{-1}}$ [7], $1.07 \times 10^{-5}\ \mathrm{m^2 \cdot s^{-1}}$ and $7800\ \mathrm{kg \cdot m^{-3}}$ [8], respectively. The value of the thermal diffusivity of molten nickel ($1.07 \times 10^{-5}\ \mathrm{m^2 \cdot s^{-1}}$) at 1828 K was obtained from the experimental data [5]. The normalized resolution of time, Δt^+, is 1×10^{-5}. The partitioned numbers n and m are 300 and 100, respectively. By this calculation condition, the convergence of the solution could be achieved. Temperature response curves reach a maximum by transmitting heat, and after that, become attenuation curves by radiation and conduction. The thermal diffusivity of molten metals could be obtained by comparing the measured temperature response curve with the theoretical one calculated by a finite difference equation. On the other hand, information on the thermal contact resistance, R, and thermal emissivity, ε, of the surface of the molten metal is very limited. Their values are also changed considerably by the experimental conditions. Thus, it is very difficult to provide at the present

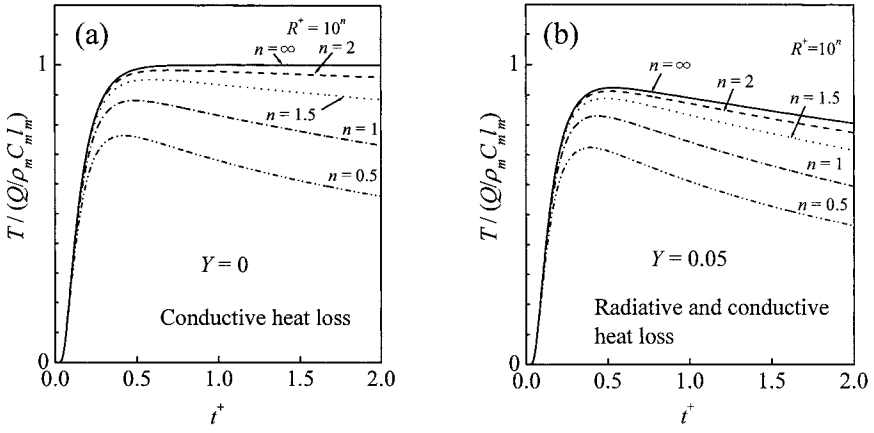

Fig. 3. Theoretical temperature response curves considering (a) conductive heat loss and (b) radiative and conductive heat loss for case of $\alpha_c^+ = 0.189$, $l_c^+ = 1$, $\lambda_c^+ = 0.109$.

time a reasonable Biot number, Y, representing the contribution of the radiative heat loss and R^+ representing that of the thermal contact resistance, based on literature values. Accordingly, thermal diffusivities of molten metals α_m are considered to be obtained by using R^+ and Y as unknown parameters, in this work.

5. THERMAL DIFFUSIVITY OF MOLTEN METALS

Data processing for comparisons between theoretical and measured temperature response curves is as follows. First, dimensionless parameters are performed by the same analysis as the laser flash method, which takes into account only the radiation heat loss. The dimensionless temperature rise, $T^* = T/T_{\max}$ is shown in Fig. 4 in a logarithmic plot against dimensionless time, $t^* = t/t_{1/2}$ by using theoretical temperature response curves given in Fig. 3. When the temperature is simply reduced by the radiative heat loss, attenuation of the temperature response curve is known to give a linear relationship with a slope, k, in the long-time region. On the other hand, when the temperature reduction is generated by conductive heat loss, the temperature response curve does not show a different behavior in the attenuation. The calculated results are given in Fig. 4, plotting with a straight-line approximation in the time range of $8 \leqslant t^* \leqslant 12$ as an example. In the case of radiative heat loss only, the thermal diffusivity can be obtained by estimating the effect of heat radiation from the slope, k. In order to estimate the effect of thermal contact resistance, it is necessary to introduce another parameter in the following procedure. The slope, k, and

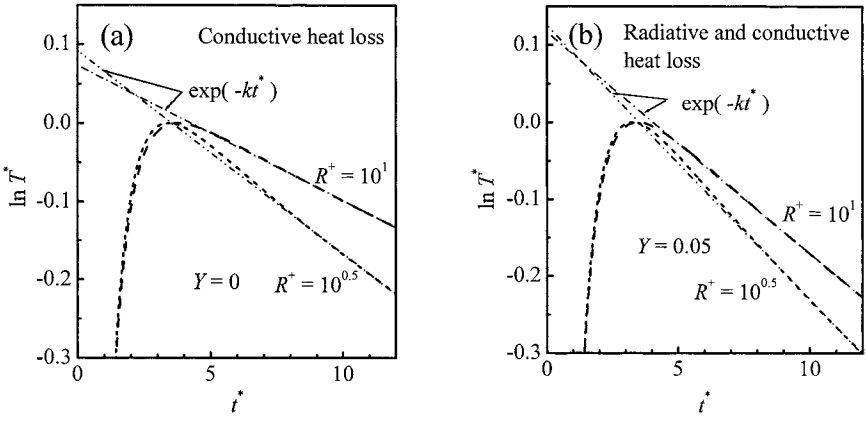

Fig. 4. Logarithmic plot of normalized theoretical temperature response curve considering (a) conductive heat loss and (b) radiative and conductive heat loss for case of $\alpha_c^+ = 0.189$, $l_c^+ = 1$, $\lambda_c^+ = 0.109$.

the intercept, $\ln T_M$, in Fig. 4 are calculated for many different values of R^+ and Y by varying the normalized thermal contact resistance in the range of $10^{0.5} \leqslant R^+ < \infty$ and the Biot number in the range of $0 \leqslant Y \leqslant 0.25$.

The relation between k and $\ln T_M$ is shown in Fig. 5. Under this condition, it is obvious that sets of R^+ and Y (R^+, Y) and sets of k and $\ln T_M$ $(k, \ln T_M)$ show one-to-one correspondence. Accordingly, (R^+, Y) can be obtained from the experimental data of $(k, \ln T_M)$. The data sets of (R^+, Y) enable us to determine the theoretical temperature response curve and the dimensionless half rise time, $t_{1/2}^+ = \alpha_m t_{1/2}/l_m^2$. In other words, where $t_{1/2}^+$ is

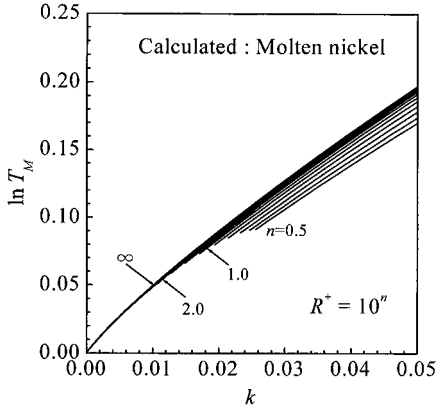

Fig. 5. Relationship between k and $\ln T_M$ for calculated results for molten nickel.

equal to K, the thermal diffusivity of molten metals can be calculated from $t_{1/2}$ by Eq. (A5) (see Appendix).

An iterative calculation is required because R^+, Y, α_c^+, and λ_c^+, which are necessary to calculate the theoretical temperature response curve, depend on α_m. The following data analysis is used to determine thermal diffusivity values in this work.

1. Values of $\langle t_{1/2} \rangle$, $\langle k \rangle$, and $\langle \ln T_M \rangle$ and are obtained as follows, where $\langle\ \rangle$ indicates a value derived from the measured temperature response.
   (a) The maximum value of the temperature $\langle T_{\max} \rangle$ and $\langle t_{1/2} \rangle$ are obtained from the measured temperature response curve, $\langle T(t) \rangle$.
   (b) The normalized temperature response curve $\langle T^*(t^*) \rangle$ is obtained by reducing the temperature and time of temperature response curve by $\langle T_{\max} \rangle$ and $\langle t_{1/2} \rangle$.
   (c) The normalized temperature response curve $\langle T^*(t^*) \rangle$ is converted to logarithmic values, $\ln \langle T^*(t^*) \rangle$.
   (d) From the decay part of the temperature response curve, $\ln \langle T^*(t^*) \rangle$ in the normalized time, t^* between 8 and 12, the slope, k and the intercept, $\langle \ln T_M \rangle$ for the following equation are obtained by least-squares estimation.

$$\ln \langle T^*(t^*) \rangle = \langle \ln T_M \rangle - \langle k \rangle \langle t^* \rangle \tag{29}$$

2. For the first estimated value for the iteration, the thermal diffusivity of the molten metal, α_m, is obtained from values of k and $t_{1/2}$ without considering conductive heat loss to the cell as described in the method in the Appendix.
3. α_c^+, l_c^+, and λ_c^+ are calculated from α_m, the specific heat, the density, and the size of the cell.
4. A table of theoretical values of k, $\ln T_M$, and K is obtained by the following process.
   (a) The theoretical temperature response curve is calculated with values of R^+, Y, α_c^+, l_c^+, and λ_c^+ from Eqs. (20) to (28).
   (b) $T_{\max}$ and $t_{1/2}$ are obtained from the theoretical temperature response curve. The value of K is equal to $t_{1/2}$.
   (c) A logarithmic plot of $\langle T(t) \rangle$ in the range of $8 < t^* < 12$ is performed by the same dimensionless operation for the measured temperature response curve. The slope, k, and the intercept, $\ln T_M$, are obtained by a least-square method.

Table I. Selected Values of k, $\ln T_M$, and K for R^+ and Y Derived from the Theoretical Temperature Response Curve

	Y								
	0.05			0.1			0.2		
R^+	k	$\ln T_M$	K	k	$\ln T_M$	K	k	$\ln T_M$	K
$10^{0.5}$	0.0358	0.125	0.121	0.0451	0.155	0.119	0.0623	0.207	0.114
10^{1}	0.0288	0.117	0.127	0.0397	0.155	0.124	0.0597	0.221	0.119
$10^{1.5}$	0.0200	0.0890	0.130	0.0317	0.132	0.127	0.0530	0.206	0.121
10^{2}	0.0156	0.0724	0.132	0.0276	0.118	0.128	0.0495	0.195	0.122

5. This table (Table I) presents results that can be regarded as discretized values for the continuous function K against k and $\ln T_M$. $K(\langle k\rangle, \langle \ln T_M\rangle)$, corresponding to measured temperature response curves, are calculated as follows.
   (a) Each K in Table I is regarded as a function of k. $K(\langle k\rangle)$ is obtained by interpolation of k.
   (b) Each $\ln T_M$ in Table I is regarded as a function of k. $\ln T_M(\langle k\rangle)$ is obtained by interpolation of k.
   (c) $K(\langle k\rangle)$ in $(K(\langle k\rangle), \ln T_M(\langle k\rangle))$ obtained is regarded as a function of $\ln T_M(\langle k\rangle)$. $K(\langle k\rangle, \langle \ln T_M\rangle)$ is obtained by interpolation of $\ln T_M(\langle k\rangle)$.
6. Thermal diffusivity α_m is obtained with $K(\langle k\rangle, \langle \ln T_M\rangle)$ by Eq. (A5) (see Appendix).
7. Iterative calculations for operations 3 to 6 are performed, until α_m converges.

6. RESULTS AND DISCUSSION

The temperature response curve for molten nickel at 1848 K is shown in Fig. 6 and logarithmic plot of normalized that is shown in Fig. 7. The simulated results of the relationship between k and $\ln T_M$ compared with the experimental results of molten nickel are also given in Fig. 8. It is found that the experimental results of k and $\ln T_M$ for molten nickel are concentrated near the curve of $R^+ = \infty$. Small dispersion is caused by fluctuations detected in the signal-to-noise ratio in the temperature response curves. Accordingly, the results of Fig. 8 clearly suggest that the effect of the conductive heat loss at the interface between the molten metal sample and cell

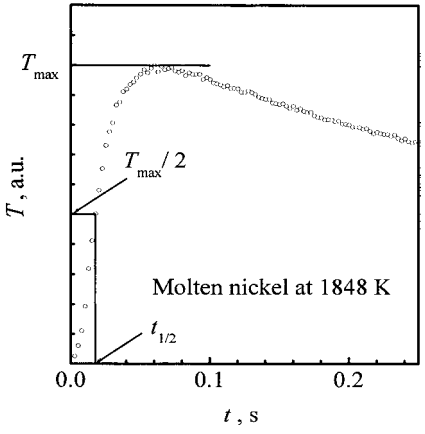

Fig. 6. Temperature response curve for molten nickel at 1848 K.

material on the temperature response curve is small in comparison with the radiative component, within the present experimental conditions.

Good reproducibility of the experimental thermal diffusivity data of molten nickel was confirmed by doing the measurements four times at a given condition (see Fig. 9). The results of Fig. 8 show the linear relationship of thermal diffusivity for molten nickel as a function of temperature, and its standard deviation is estimated to be 1.75×10^{-7}. Then, the thermal

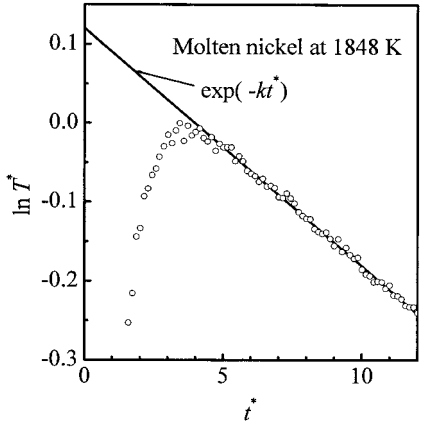

Fig. 7. Logarithmic plot of normalized temperature response curve for molten nickel at 1848 K.

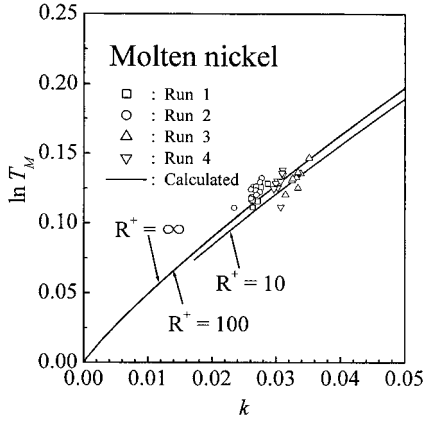

Fig. 8. Calculated relationship between k and $\ln T_M$ compared with experimental results of molten nickel.

diffusivity values of molten nickel can be described by the following equation, where α is in $m^2 \cdot s^{-1}$ and T is in K.

$$\alpha = 6.61 \times 10^{-9}(T - 1728) + 1.02 \times 10^{-5} \tag{30}$$

The thermal diffusivity value of molten nickel at the melting point (1728 K) is found to be 36% smaller than that of solid nickel at 1500 K

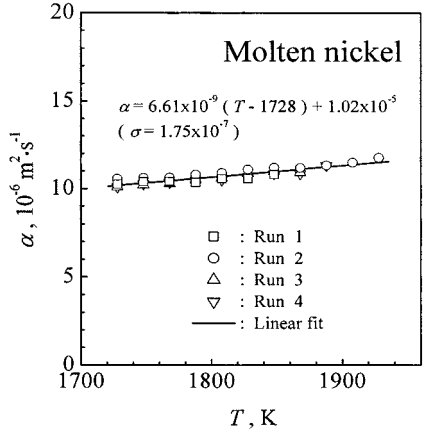

Fig. 9. Thermal diffusivity of molten nickel as a function of temperature obtained in this work.

[4]. Of course, such a distinct difference in the thermal diffusivity value is attributed to a change in the structure from the atomic distribution with periodicity to that with no periodicity at melting. It may also be worth noting that the thermal diffusivity values of molten nickel show a slightly positive temperature dependence, although its origin cannot be identified at the present time. It should also be noted from the present analysis described in Section 5, that the uncertainty of the thermal diffusivity of molten nickel is $\pm 3\%$ in comparison with thermal diffusivity values obtained considering only the effect of radiative heat loss. Moreover, the thermal diffusivity value of molten nickel at 1928 K is 6.7% smaller than the value derived without considering the radiative heat loss.

7. CONCLUSION

The thermal diffusivity of molten nickel was determined by calculating and measuring the temperature response curves of the laser flash method. The results are summarized as follows.

(1) Considering both the radiative and conductive heat losses from a molten metal sample to the cell, the calculated temperature response curves are obtained for the numerical model. The thermal diffusivity of molten nickel was determined from the calculated temperature response curves.

(2) The uncertainty of the thermal diffusivity of molten nickel is $\pm 3\%$ in comparison with thermal diffusivity results obtained considering only the effect of radiative heat loss.

(3) The usefulness of a cell for the newly developed laser flash method has been analyzed, and it would be interesting to extend the simulated results to evaluate the heat leakage in the thermal diffusivity measurement of molten metals.

APPENDIX

When only the radiative heat loss is taken into account to obtain the thermal diffusivity, the temperature response curve for the bottom of the molten metal changes according to the following equation:

$$T = \frac{Q}{\rho_m C_m l_m} \sum_{n=0}^{\infty} A_n \exp(-X_n^2 t^+) \tag{A1}$$

where Q (see Fig. 2) is the total energy absorbed by the molten metal, ρ_m is the density of the molten metal, and C_m is the heat capacity of the molten metal.

$$A_n = 2(-1)^n X_n^2 (X_n^2 + 2Y + Y^2)^{-1} \tag{A2}$$

$$X_0 = (2Y)^{1/2} (1 - Y/12 + 11Y^2/1440) \tag{A3}$$

for $n \geqslant 1$

$$X_n = n\pi + 2Y/(n\pi) - 4Y^2/(n\pi)^3 + \{16/(n\pi)^5 - 2/[3(n\pi)^3]\} Y^3 + \{-80/(n\pi)^7 + 16/[3(n\pi)^5]\} Y^4 \tag{A4}$$

Equation (A1) is plotted in Fig. 10. When the radiative heat loss from the molten metal surface is taken into account, the thermal diffusivity of the molten metal, α_m is obtained with the following equation [9].

$$\alpha_m = K \frac{l_m^2}{t_{1/2}} \tag{A5}$$

where K is the coefficient determined theoretically by the ratio of the radiative heat loss to the conductive heat flux, and the value of K becomes 0.1388 at adiabatic conditions where the heat loss is negligibly small [10]. $t_{1/2}$ is the time required for the back surface of the sample to reach one half of the maximum temperature rise.

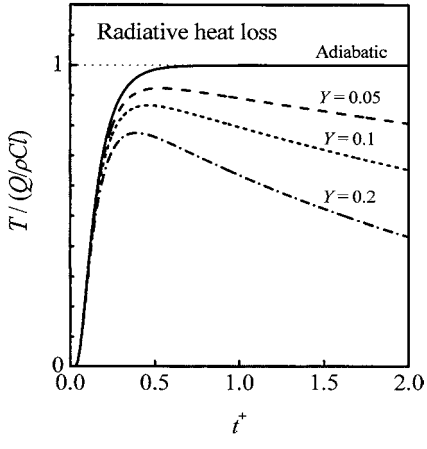

Fig. 10. Theoretical temperature response curves considering radiative heat loss.

In order to estimate the value of K, the following procedure was conducted. When the radiative heat loss becomes significant, the temperature of the back surface of the sample reaches its maximum and decreases along the line proportional to the following equation:

$$T = \frac{Q}{\rho_m C_m l_m} A_0 \exp(-X_0^2 t^+) \tag{A6}$$

Time and temperature rise are normalized using $t_{1/2}$ and the maximum temperature rise, T_{max}. The normalized time is defined as $t^* = t/t_{1/2}$ and the normalized temperature rise is defined as $T^* = T/T_{max}$. When T^* is plotted logarithmically against t^* (see Fig. 11), Y can be obtained from the slope of the logarithmic attenuation, $k = d \ln T^*/dt^*$. In addition, if Y is determined, K can be obtained. Ohta et al. [11] reported the coefficient K in the range between $k = 0$ and 0.40. The coefficient of K can be given in the following form as a function of k.

$$K = 0.1388 - 0.3873k + 1.369k^2 - 3.223k^3 + 2.805k^4 \tag{A7}$$

In practice, k is determined, in the first step, from the measured temperature response curve in the longer time region and, subsequently, we obtain the K value with the obtained value of k from Eq. (A7) and thus the thermal diffusivity value of molten metal is obtained from Eq. (A5).

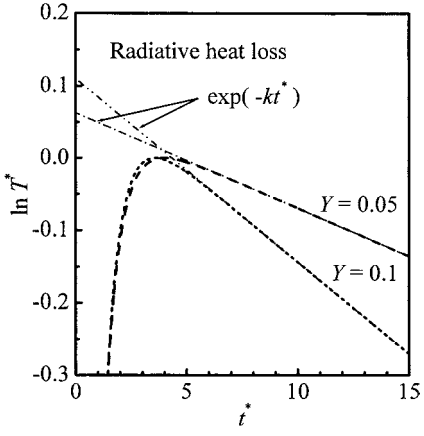

Fig. 11. Logarithmic plot of normalized theoretical temperature response curve considering radiative heat loss.

ACKNOWLEDGMENT

This work is supported by Special Coordination Funds for Promoting Science and Technology (Promotion System for Intellectual Infrastructure of Research and Development, "Research on measurement technology and reference materials for thermophysical properties of solids"), Japan and a Grant-in-Aid for Scientific Research (13750683-00) of the Ministry of Education, Culture, Sports, Science and Technology, Japan.

REFERENCES

1. J. T. Schriempf, *High. Temp. High. Press.* **4**:411 (1972).
2. B. J. Monaghan and P. N. Quested, *ISIJ Int.* **41**:1524 (2001).
3. NPL REPORT CBTLM **S30** (2000).
4. Y. S. Touloukian, R. W. Powell, C. Y. Ho, and M. C. Nicolaou, in *Thermophysical Properties of Matter*, Vol. 10 (IFI/Plenum, New York, 1973), pp. 48, 51, 82, 120.
5. T. Nishi, H. Shibata, H. Ohta, and Y. Waseda, *Metall. Mater. Trans. A* **34** (2003), in press.
6. *Handbook of Thermophysical Properties*, ed. by ISTP, Yokendo, Tokyo (1990), p. 260 [in Japanese].
7. *Handbook of Molten Steel and Slag*, ed. by ISIJ, ISIJ, Tokyo (1971), pp. 178–181 [in Japanese].
8. T. Saitoh, M. Amatatsu, and S. Watanabe, *Bull. Res. Inst. Miner. Dressing Metall., Tohoku University* **25**:67 (1969) [in Japanese].
9. Y. Takahashi, T. Azumi, and M. Sugano, *Netsu-Sokutei* **8**:62 (1981) [in Japanese].
10. W. J. Parker, R. J. Jenkins, C. P. Butler, and G. L. Abbott, *J. Appl. Phys.* **32**:1679 (1961).
11. H. Ohta and Y. Waseda, *High. Temp. Mat. Proc.* **7**:179 (1986).